A 3-D-Printed High-Dielectric Materials-Filled Pyramidal Double-Ridged Horn Antenna for Abdominal Fat Measurement System

Siamak Sarjoghian, *Member, IEEE*, Yasir Alfadhl, *Senior Member, IEEE*, Xiaodong Chen, *Fellow, IEEE*, and Clive G. Parini, *Member, IEEE*

***Abstract*— This article presents a novel 3-D-printed, pyramidal double-ridged horn antenna, filled with a high-dielectric material comprising a mixture of linseed oil and titanium oxide, for biomedical applications. In particular, this investigation explores the use of the antenna design to measure the abdominal fat layers of the human body. The antenna is designed to operate at the low-frequency microwave bands and complemented with an absorber layer at the aperture to improve directivity. The proposed method aims to assess the fat layer thicknesses based on an analysis of the variations of the reflection coefficients. The system has been calibrated and validated based on a number of numerical time-domain simulations, as well as experimental analysis. Assessment of the first transition point in the reflection coefficient spectrum has successfully predicted the rate of magnitude change caused by different layer thicknesses (e.g., oil and fat). Comparing coefficient spectra from various simulation experiments has allowed for eliminating the interferences arising from mismatches with the skin and muscle layers, resulting in the measurements of the fat layer thicknesses through the remaining power change rate.**

***Index Terms*— 3-D printing, abdominal fat, antenna, double-ridged horn, high-dielectric material.**

I. Introduction

A PYRAMIDAL double-ridged horn (PDRH) antenna was first introduced in 1964 [1], although the concept of the ridged-waveguides was introduced earlier in 1947 [2]. This type of antenna was utilized for biomedical applications by various research groups to monitor the inside of the human body [3], [4]. This antenna has attracted many other engineers and researchers in the radar field, due to its advantages such as large bandwidth, high gain/directivity, and matching capability [5], [6].

These important principles make this type of antenna an efficient solution, as compared with other bidirectional antenna types, such as the Bowtie [7], Vivaldi [8], and wire helix antennas [9]. However, in contrast to these advantages, the antenna suffers from some disadvantages, such as high fabrication cost, and a large aperture for the low-frequency applications (i.e., 1–3 GHz).

Manuscript received December 10, 2018; revised October 17, 2019; accepted June 12, 2020. Date of publication July 16, 2020; date of current version January 5, 2021. *(Corresponding author: Siamak Sarjoghian.)*

The authors are with the School of Electronic Engineering and Computer Science, Queen Mary University of London, London E1 4NS, U.K. (e-mail: s.sarjoghian@qmul.ac.uk).

Color versions of one or more of the figures in this article are available online at https://ieeexplore.ieee.org.

Digital Object Identifier 10.1109/TAP.2020.3008653

The latter is of crucial demand in scanning human body applications due to the penetration depth factor [10]. In order to overcome the cost of fabrication, a different type of 3-D printing technique was developed and proposed by engineers, which use different materials such as metal and plastic [11], [12].

Although 3-D metal printing is currently practiced in parts of the industry, as it is known to be costly. Moreover, the surface of the fabricated design using the material is relatively rough, which can reduce the antenna design band [13]. Therefore, in-house 3-D printing using plastic has been selected as an optimal alternative solution concerning the cost as well as the ease of fabrication [12].

Different studies have also employed this type of fabrication method [14], and consequently, a diverse set of solutions have been provided to overcome the technical complications. As such, in order to uniformly paint the internal facets of the structure, and to further smooth the rough surface (i.e., generated during the 3D printing), the antenna was cut from the middle into two separate parts, which were screwed back together after being painted. The latter also resulted in the improvement of the surface conductivity. The bulky structure of the PDRH antenna in a system and the large reflections (to be eliminated) due to environmental mismatch are other concerns of this design. Recent studies have shown that in order to solve this issue, high-dielectric and low-conductive materials are embedded within the antenna structure; e.g., ceramics, oil, and pure water [15]–[17].

Various challenges such as fabrication complications, high cost, and high conductivity have been addressed to finalize a viable design of the material-embedded antenna [18]. In the case of ceramics, the cost of such a high-dielectric one, as well as the fabrication method, have made researchers think of other solutions, such as pure water that has a low conductivity due to the elimination of particles in water. Following an extended investigation on the use of distilled and deionized water types (i.e., the water molecule structure and high conductivity even after particle elimination), it was concluded that majority of input power becomes absorbed within the antenna structure [17]. Consequently, oil was defined as the optimal liquid solution, due to its low conductivity, although oils are associated with low permittivity [19].

Early diagnostics of fat inside the human body, especially underneath the skin, is an important factor for diagnosing other

associated diseases [20]. Medical practitioners to liposuction or other types of procedures on patients also need fat-thickness detection. In current practices, various assessment techniques are used, such as waist measurement in the general practitioners [21], magnetic resonance imaging (MRI) method [22], computed tomography (CT) method [23], [24], and ultrasound [25]. Each of these methods has its own sets of drawbacks, such as accuracy, errors, radiation hazards, and cost.

The aim of this work is to design, develop, and implement a low-cost portable system that is capable of measuring the thickness of abdominal fat layer underneath the human skin (i.e., subcutaneous fat) that could relate to the internal fat (i.e., visceral fat) to monitor the health. The wideband (WB) term developed here denotes partial utilization of the free band (3.1–10.6 GHz) provided by the federal communications commission (FCC) for ultra-wideband (UWB) part of the spectrum [10]. The WB spanning between 1 and 3 GHz was selected as a term for the antenna design based on its unique features, which further propose inexpensive solutions due to low-power consumption pulses and the propagation characteristics within the human tissue.

The main contributions of this work can be summarized as follows.

1) Novel compact PDRH antenna has a shape and fabricated process that not only comforts the finalized system, but also improves the operation, e.g., directivity, gain, and bandwidth to some extent compared to the similar designs.
2) Unique application of semisolid high dielectric material with the low conductivity was used to miniaturize the design and reduce the reflection within the system. Moreover, the material has advantages, e.g., elimination of the air gaps may develop when the antenna was placed on the human body as well as easy and low cost to manufacture into the required shape.
3) The absorber sheet was employed at the extension point of the design in order to not only reduce the mismatched caused by the extended plastic; moreover, it could significantly improve the design directivity.
4) The evaluation of the reflection coefficient (S11) results of the antenna design at the lowest frequency (i.e., 1.8 GHz), where the design has the highest penetration capability was proposed and proved as a suitable technique to measure the human fat thickness.

The rest of this article is organized as follows. Section II covers the materials characterization and associated methods. Section III presents the comprehensive analytical and numerical design and performance evaluation of the developed antennas based on the deployed RF technologies. Section IV shows the experimental stages that present the fabrication process, and the prepared set up for the measurements on the liquid models and the human body. Section V concludes this article.

II. Materials Characterization

Different types of high-dielectric and low-conductive materials and their mixtures have been developed for the proposed system, which aims to monitor inside the human body. In this regard, the oil, such as canola oil, was of interest due to its low conductivity, low cost, and safety for skin-centric biomedical applications [19]. The open-ended coaxial probe method, which is well established in the literature as one of the principal methods for liquid dielectric measurement, has been applied to characterize the developed materials. The dielectric measurement setup comprised a vector network analyzer (VNA) Agilent PNA-L—N5230C (0.01–20 GHz), dielectric probe (25 mm diameter), and Agilent electronic calibration (ECal) module. All measured samples were stabilized at 20 °C during all the experimental measurements. The VNA (i.e., PNA-L), ECal kit, and open-ended probe setup are shown in Fig. 1. The instruments were calibrated with the distilled water presented in Fig. 2(a) and (b) to increase the system's accuracy. Measurements were carried out on different types of oils, such as linseed, olive, avocado, pig, duck, and salmon ones. The measured dielectric properties of the measured samples at 1.8 GHz are demonstrated in Table I. The results indicate that linseed oil has the highest permittivity among the experimental oils with low satisfactory conductivity. Fig. 2(a) and (b) present the permittivity and conductivity of the linseed oil measured using the probe method in the range of 0.3–3.3 GHz.

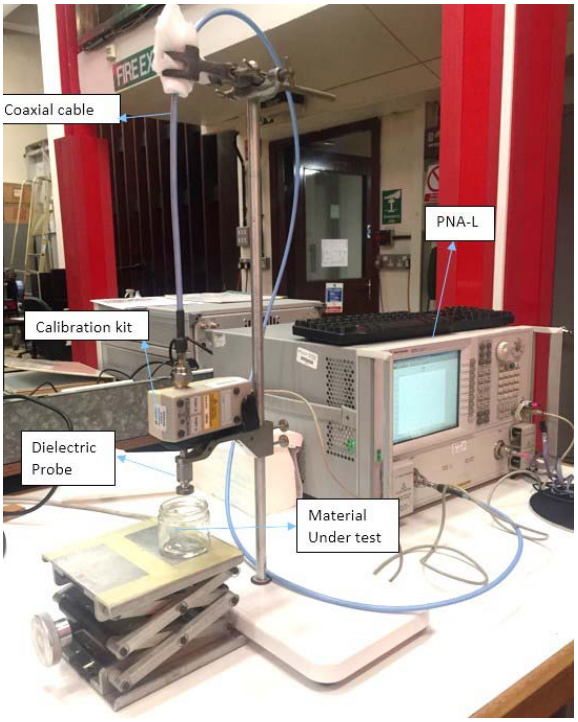

Fig. 1. Open-ended coaxial probe technique deployed for the measurement of the dielectric materials.

Titanium oxide (TiO_2) powder has been used widely in different products, such as sun creams and high dielectric ceramics [26]. The measured sample of the TiO_2, after it is sintered using the spark plasma sintering (SPS) method, demonstrates that it can maintain low conductivity and high-dielectric constant ($\varepsilon_r \sim 86.7$ at 1.8 GHz) shown in Fig. 2(a).

Based on these results, the ceramic powder has been chosen as a candidate to be mixed with the linseed oil, to increase the permittivity of the material. Hence, different portions of each

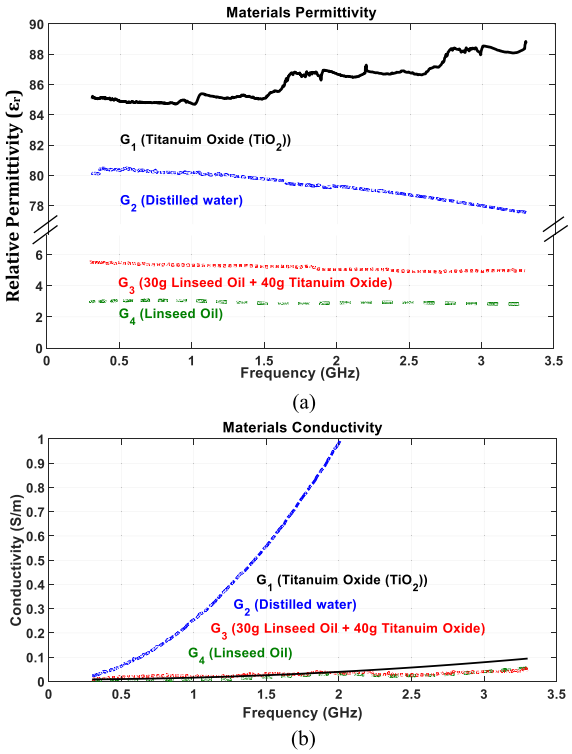

Fig. 2. (a) Measured permittivity of water, TiO_2, linseed oil, and their proposed mixture at 0.3–3.3 GHz. (b) Measured conductivity of water, TiO_2, linseed oil, and their proposed mixture at 0.3–3.3 GHz.

TABLE I

MEASURED DIELECTRIC PROPERTIES OF DIFFERENT TYPES OF OILS AT 1.8 GHPz USING THE OPEN-ENDED PROBE TECHNIQUE

Dielectric Material	Frequency (GHz)	Relative Permittivity	Conductivity (S/m)
Linseed oil	1.8	2.87	0.027
Olive oil	1.8	2.75	0.023
Avocado oil	1.8	2.72	0.025
Salmon oil	1.8	2.75	0.025
Duck oil	1.8	2.49	0.020
Pig oil	1.8	2.20	0.007

material have been mixed and the dielectric properties were measured and represented in Fig. 2(a) and (b).

The ideal four portions of the TiO_2 (40 g) mixed with three portions of the linseed oil (30 g) have produced a flexible homogenous material, with the given measured dielectric properties as shown in Fig. 2(a) and (b), using the open-ended probe method in the range of 0.3–3.3 GHz. The measured permittivity of the mixture has been almost twice than of linseed oil ($\varepsilon_r \sim 5.26$ at 1.8 GHz) with higher conductivity.

It was noticed that dielectric measurements at higher frequencies had suffered certain irregular fluctuations. This was attributed to the unavoidable small air gaps between the sample and probe. These fluctuations were more evidential in the case of the solid sample TiO_2 due to the increased volume of air gap between the solid sample and the probe. These small air-gap errors are related to resonances due to mismatch and are minimal at lower frequencies due to lower resolution as it increases at higher frequencies, as it is expected [18].

This high-dielectric mixture has been proposed here to be embedded within the antenna design, which is being also used later in the proposed system. The main objective of using such a high dielectric material in a radar-centric system, which also operates on a human body, is to reduce the size of the antenna, to eliminate the reflections due to mismatching environment, and to form a flexible case of embedding material for a specific antenna structure. Moreover, when the antenna has been placed on the body, the liquid form of this mixture at the surface is able to fill in the air gaps that may exist between the antenna and the skin that also results in a better impedance network matching.

III. ANTENNA DESIGN AND EVALUATIONS

The horn antenna is considered as one of the most universal microwave antennas in technical deployment for many years [27]. Moreover, among different types of horn antennas, the PDRH has attracted researchers in the medical imaging domain, due to desirable factors, such as network matching capability, design simplicity, ease of excitation, and high bandwidth and gain [28]. The fabrication and miniaturization of such a design are considered as the main challenges of the system [15], [29].

A. Antenna Design and Analysis

The main target of this work is to provide a solution to overcome the limitations of a PDRH antenna that can be employed to measure the abdominal fat. The use of the proposed high-dielectric mixture has resulted in efficient miniaturization and resolving matching issues. Regarding the fabrication and realization, the method of 3-D printing has been performed using the transparent polyethylene material to effectively reduce the costs and the fabrication complexity.

The extension is proposed to place the antenna close to the far-field region, in order to excite the plane wave into the monitoring area and to produce a delay to eliminate the reflections overlapping issue [18]. An antenna in the free-space has the wave impedance of 377 Ω, where if the antenna is built or immersed in any dielectric material, the impedance would be different and can be defined as follows [19]:

$$z_m = \sqrt{\frac{\mu_0}{\varepsilon_0 \varepsilon_r}} \tag{1}$$

where $\varepsilon_0 = 8.854 \times 10^{-12}$ (F/m), and $\mu_0 = 4\pi \times 10^{-7}$ (V.s/A.m) are the permittivity and permeability of free space, and ε_r is the relative permittivity of the dielectric material that aims to fill the antenna to reduce the size and to eliminate bulky reflections, as a result of the dielectric mismatch.

Moreover, the permittivity of the medium where the antenna operates inside is considered during the design process to achieve the highest performance [19].

The proposed medium for the antenna has a permittivity of 5.1 at 1.8 GHz; hence, the impedance of the medium could

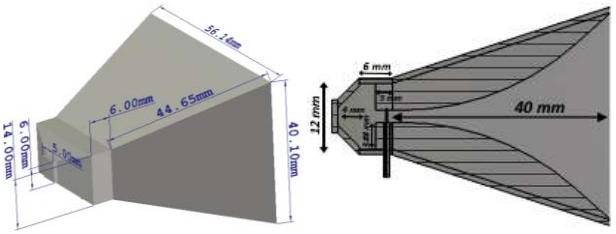

Fig. 3. Modeled PDRH antenna, with the aperture dimensions.

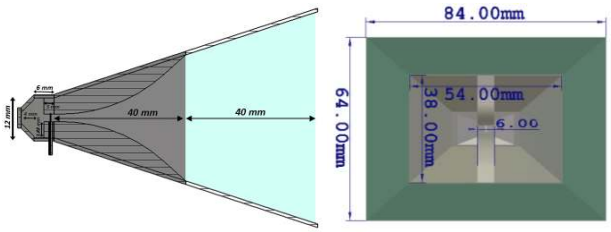

Fig. 4. Modeled extended PDRH antenna, with the aperture dimensions.

be defined using (1) as 167.7 Ω; i.e., reduced by less than half compared to the free-space.

The exponentially tapered section of the antenna is very important as it matches the reference impedance in the feeding point of the device, to that of the material at the aperture, which is varying from 50 to 167 Ω and is obtained as follows:

$$z(y) = z_0 e^{ky}, \quad (0 \le y \le L) \tag{2}$$

where y is the distance from the waveguide aperture, and L is the axial length to the opening of the exponentially tapered section; k is determined by [30], [31]

$$k = \frac{1}{L} ln\left(\frac{Z_L}{Z_0}\right) \tag{3}$$

where Z_L and Z_0 are the characteristic impedances of the double-ridged waveguide in the medium and free-space, respectively.

The dimensions of the E- and H-planes of a pyramidal horn have been determined based on the dielectric material and the equations presented in the seminal antenna textbook [32]. The antenna design has been based on the calculated parameters and modifying them in order to operate within the desired frequency of operation sets in the CST Studio [33].

Fig. 3 presents the modeling of the proposed antenna based on the measured materials mixture (i.e., linseed and TiO_2) loaded into the software as new material by using the user dispersion option, and the robust transient time-domain solver.

In order to achieve the objective of the system, and to avoid pulses (transmitted and reflected) overlapping issues, a tapered dielectric extension has been added to the main antenna structure. Simulations have demonstrated that this can be achieved with extensions with lengths equal or bigger than the flared aperture, as shown in Fig. 4. Therefore, an extension equal to the flared aperture was added to the design to generate a physical delay between the transmitted pulse and reflected pulse to avoiding overlapping issues.

Moreover, the technique locates the antenna close to the middle or far-field region for a better pulse propagation into the monitoring area. In general, it was concluded that the introduced tapered dielectric extension has made the device more operationally stable and free of any destructive interference signals and noise [18].

The high-dielectric PDRH antenna has been extruded with the pyramidal aperture length of 40 mm, based on the following equations, in order to maintain the primary design antenna objectives. In addition, to define the outer aperture of this extended part, when the length of the extension changes,

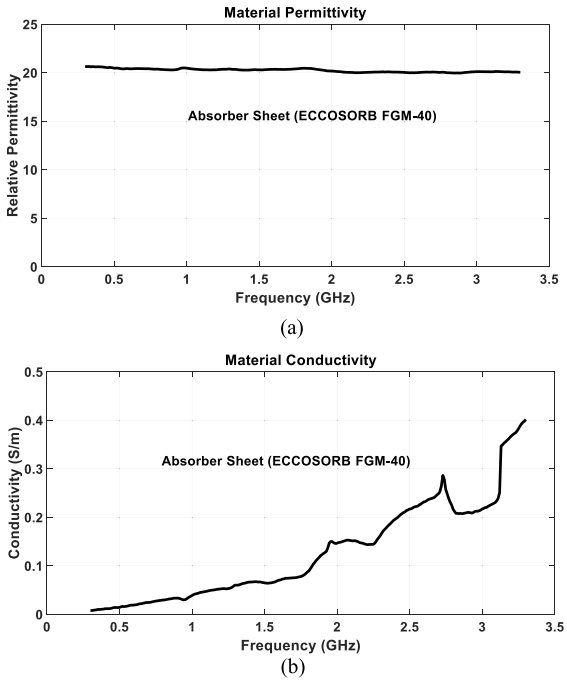

Fig. 5. (a) Measured permittivity of the absorber at 0.3–3.3 GHz. (b) Measured conductivity of the absorber at 0.3–3.3 GHz.

the following equations have been derived:

$$w_{a2} = 2 \times \left[\frac{w_{a0}}{2} + \frac{w_{a1} - w_{a0}}{2 \times l_1} \times (l_2 + l_1)\right] \tag{4a}$$

$$w_{b2} = 2 \times \left[\frac{w_{b0}}{2} + \frac{w_{b1} - w_{b0}}{2 \times l_1} \times (l_2 + l_1)\right] \tag{4b}$$

where w_{a2}, w_{b2}, and l define the width, height, and length of the horn aperture, respectively, and are represented in Fig. 4.

A thin, flexible, and magnetically loaded silicone microwave absorbing material sheet (i.e., ECCOSORB FGM-40) has been selected to be employed as part of the high-performance design of the proposed antenna [34]. The measured dielectric properties of this absorbing sheet have been loaded into the simulation software presented in Fig. 5(a) and (b) to validate the findings. The absorber has the approximate measured dielectric constant of 20, and the conductivity that rises over the desired frequency range to 0.4 S/m (0.3–3.3 GHz). The developed mixed material was chosen as the background material in the simulation, to evaluate the performance inside the medium. As such, the figures of merit for the evaluation of the proposed antenna with and without absorber sheet,

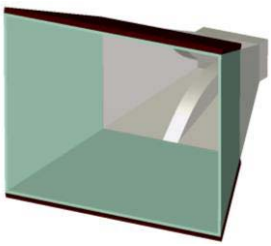

(a)

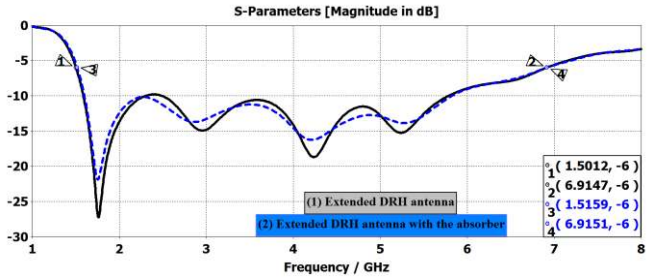

(b)

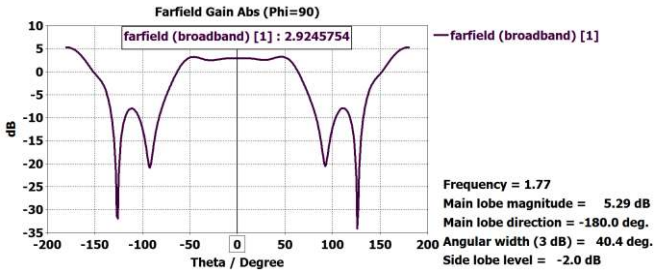

(c)

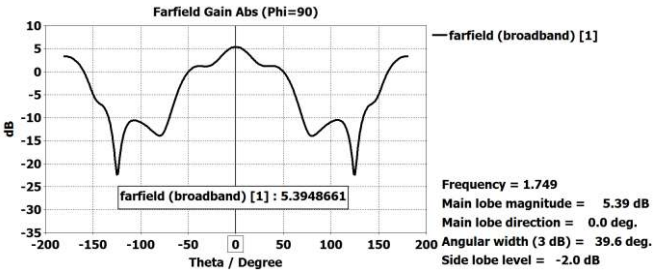

(d)

Fig. 6. (a) Extended PDRH antenna with the absorber sheets placed on top and bottom of the extended aperture. (b) Simulated S_{11} when the antenna is inside the proposed material with and without the absorber sheet attached to the extended part. (c) Cartesian EM far-field radiation pattern of the antenna, without the absorber, at 90° at the transition point (1.763 GHz). (d) Cartesian EM far-field radiation pattern of the antenna, with the absorber, at 90° at the transition point (1.749 GHz).

including the reflection coefficients based on the S_{11}, gain, and radiation patterns, are obtained and shown in Fig. 6(a)–(d).

The reflection coefficients shown in Fig. 6(b) depict the wide operating bandwidth of 5.4 GHz from 1.5 to 6.9 GHz, taking the value of −6 dB as a reference; i.e., commonly set for the on-body applications [19]; and the large transition at a low frequency of 1.77 GHz. Fig. 6(c) shows the radiation patterns, in Cartesian, and the gain at the transition points (1.77 GHz).

This shows the gain of 2.92 dB in the zero degree at the front-end and the gain of 5.29 dB at the back-end, due to the extended part that is filled with a high-dielectric material, which is used as the background material in the simulation.

Balegh *et al.* [35] have proposed to utilize an absorbing sheet of graphene in the lower and upper flare extensions to reduce the sidelobe levels (SLLs), and hence, increasing the antenna directivity. The absorber sheet has been modeled in the modeling software, based on the measured data.

Two sheets have been attached to both the lower and upper outer extended flares of the antenna where the design flare sections joint with the extended plastic. These sections are the locations of the ridges, which the wave is propagating through, as in Fig. 6(a).

Moreover, Fig. 6(b) shows that the effects of the absorber on the operating frequency is negligible, due to a minor frequency shift for the first large transition point ∼20 MHz, and a slight increase in the bandwidth ∼10 MHz. However, the far-field radiation pattern presents a significant effect on the directivity and gain, as in Fig. 6(d). The gain is increased to 5.39 dB, and SLLs are further reduced, exhibiting an improved directivity, compared with the case without the absorber.

TABLE II

DIFFERENCE IN THE FREQUENCY AND MAGNITUDE AT THE FIRST LARGE TRANSITION POINT, WITH A REFERENCE TO THE OIL THICKNESSES

Oil Thickness (mm)	Frequency (GHz)	Magnitude (dB)
10	1.752	–19.575
20	1.728	–21.077
30	1.712	–25.018

B. System Evaluation Using a Liquid Model

A liquid model consisting of two layers of the distilled water and linseed oil has been proposed, in replacement of the fat and muscle in the humans' tissue model, and a thin layer of skin is ignored, to approximate the performance of the system before utilizing it in the developed model.

A center frequency of 1.8 GHz was chosen to monitor the system. The dielectric properties of both the measured liquids using the discussed open-ended probe technique are shown in Fig. 2(a) and (b). The simulated antenna was placed on the liquid model, where the thickness of the oil layer was increased, from zero-thickness at first and is then increased from 10 to 30 mm, with an iteration sequence of 10 mm, as in Fig. 7(a).

The reflection coefficients (S_{11}) were recorded for each case. The method developed to employ the highest magnitude of the first largest reflection coefficient close to $f_c = 1.8$ GHz. The first S_{11} measurement has been chosen for the case when only the water exists, which is used to initiate the system calibration, as shown in Fig. 7(b).

This was followed by a set of scenarios when the oil thickness iterates and markers indicate the changes in the magnitude at the first largest transition close to the desired frequency, as in Fig. 7(c).

Table II shows the generated graph/equation that is obtained from the first highest magnitude points of the desired region for different thickness scenarios, in order to relate the rate

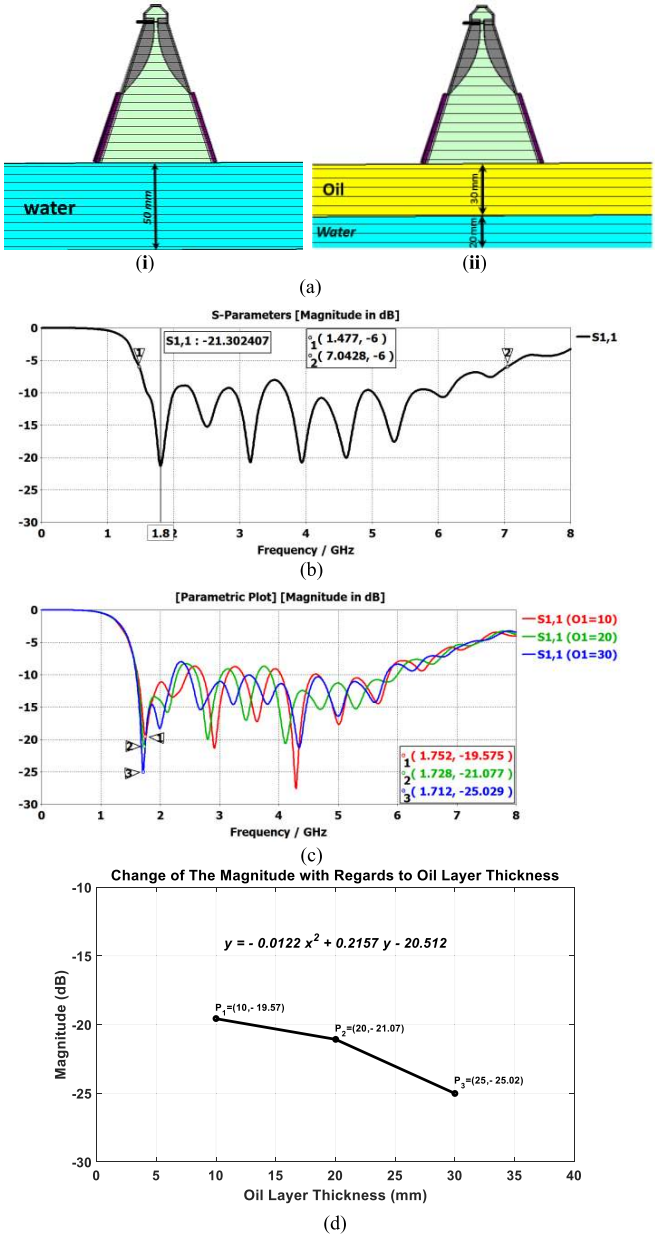

Fig. 7. (a) Modeling of the developed PDRH antenna, which is placed on: (i) distilled water and (ii) oil layer with thicknesses of 10–30 mm. (b) Simulated S_{11} of the antenna placed on the distilled water. (c) Simulated S_{11} when the oil layer thickness changes from 10 to 30 mm, with an iteration of 10 mm. (d) Generated graph and equation based on the simulated S_{11} data, presenting the rate of change in magnitude, when the oil layer thickness iterates from 10 to 30 mm in the first large transition.

of the magnitude change to that of the different oil thickness scenarios.

C. System Evaluation Using an Abdominal Tissue Model

In the next stage of design, the tissue model that consists of three layers, i.e., 2 mm skin, 15–30 mm fat, and infinite muscle; has been thoroughly developed in the software. This has been conducted to present the abdominal tissue and the antenna filled with the material mixture, which is placed on this tissue model, as shown in Fig. 8(a).

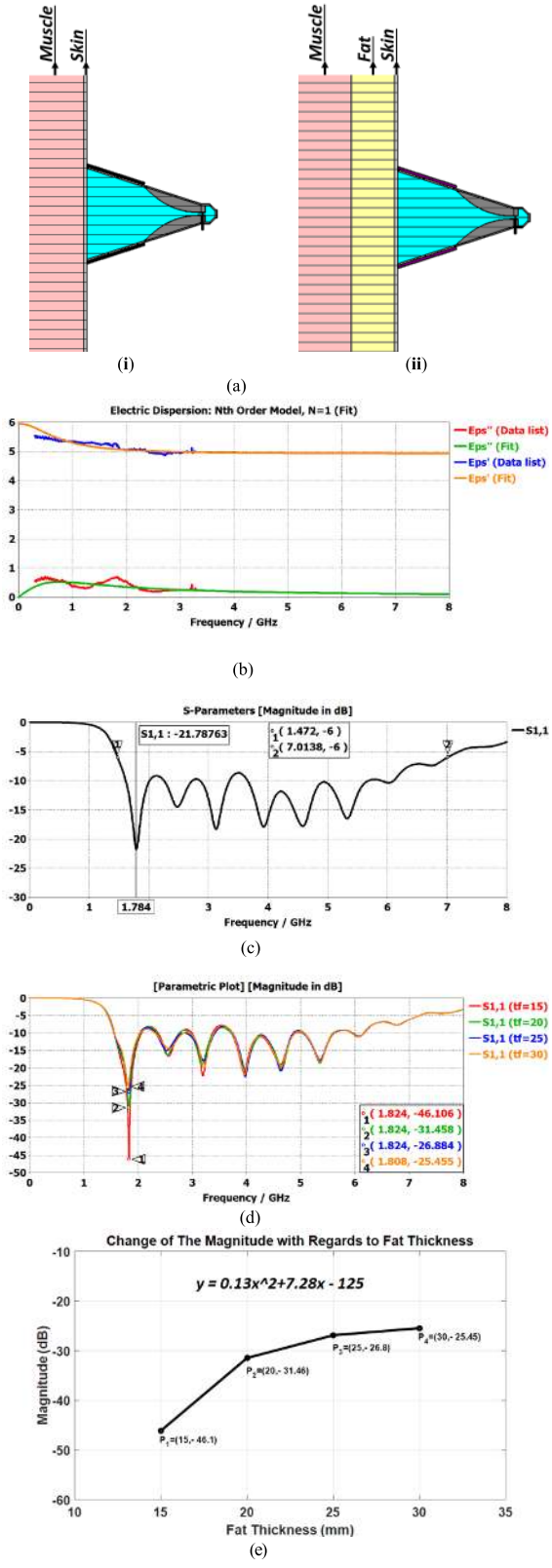

Fig. 8. (a) Modeling of the developed PDRH antenna, which is placed on: (i) tissue without the fat layer and (ii) tissue with the fat layer. (b) Measured properties of the mixture loaded into the software. (c) Simulated S_{11} of the antenna, when the fat layer does not exist. (d) Simulated S_{11} when the fat layer thickness changes from 15 to 30 mm, with an iteration of 5 mm. (e) Generated graph and equation based on the simulated S_{11} data, presenting the rate of change in the magnitude, when the fat layer thickness iterates from 15 to 30 mm in the first large transition.

TABLE III

DIFFERENCE IN THE FREQUENCY AND MAGNITUDE AT THE FIRST LARGE TRANSITION POINT, WITH A REFERENCE TO THE FAT THICKNESSES

Fat Thickness (mm)	Frequency (GHz)	Magnitude (dB)
15	1.824	–46.108
20	1.824	–31.458
25	1.824	–26.884
30	1.808	–25.455

Moreover, the dielectric properties of the material in the desired frequency region (i.e., already measured) have been also loaded into the software using the new material dispersion characteristics, as shown in Fig. 8(b).

The high-dielectric material-filled PDRH antenna was placed on the tissue model without the fat layer, and the S_{11} results are obtained for a very low-frequency range up to 8 GHz that is assumed as a calibration point shown in Fig. 8(c). The fat layer increases from 15 to 30 mm with an iteration of 5 mm and the results have been captured and depicted in Fig. 8(d).

The results demonstrate a constant change in the magnitude at the first large transition with respect to the thickness of the fat layer, as in Table III. Fig. 8(e) also shows a generated graph and an equation based on the data collected from the magnitude difference at the first large transition point, when the thickness of the modeled tissue fat layer iterates from 15 to 30 mm. The generated equation can also be used to accurately predict the fat layer based on the measured data [36].

IV. ANTENNA FABRICATION AND MEASUREMENT

A. Antenna Fabrication and Realization

Fabrication of the 3-D printed PDRH antenna required an in-house 3-D printer (Stratasys Objet30 Prime), and some modification to the design, such as cutting the designed antenna symmetrically to two parts before the printing, and allocating a screw spacing on the side edges to attach them together, as in Fig 9(a). The 3-D printer was employed in order to print the prototype with a resolution of 100 μm. This 3-D-printed prototype has been realized with a clear finish and the supportive material that is removed by rinsing the prototype using pressurized water. The cost of a Vero clear transparent polyethylene is ∼650 USD per kg [37].

Hence, the cost of the Vero material including the support material used to 3-D print the prototype is less than 50 USD. The Objet30 printer offers cost-effective solutions for 3-D printing complex structures with a high resolution. The printed PDRH antenna has been painted with silver conductive paint, up to the extended part of the design. The antenna has been connected to a 50-Ω semiridge SMA connector with an outer dimension of 1.19 mm fed and glued to the antenna's lower and upper ridges, as in Fig. 9(b).

The antenna was further filled with the TiO_2 mixture, and it was placed upside down and was well shaken in order to remove any remaining bubble gaps produced during the mixing and filling procedures, i.e., shown in Fig. 9(c) [38]. With regard to the minor air gap, the vacuum chamber can be used during the mixing and filling procedures; however, the tiny air gaps can be ignored by the antenna system at the low-frequency range [18].

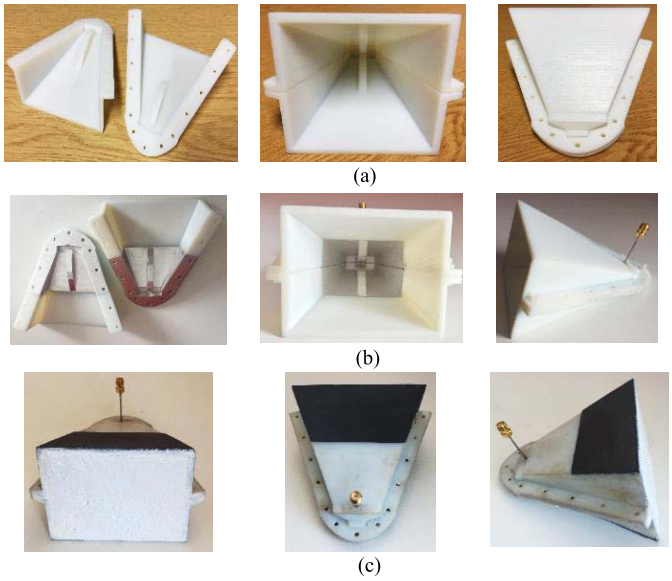

Fig. 9. (a) 3-D-printed PDRH antenna using the polyethylene material. (b) 3-D-printed PDRH antenna conductive-painted and fed with a semiridged SMA connector. (c) 3-D-printed PDRH antenna filled with the high-dielectric material and the absorbers are glued to lower and upper extended flares.

B. Experimental System Evaluation Using a Liquid Model

A two-layer liquid model consisting of a distilled water and linseed oil is developed, to validate the concept of the operation, which has been to accurately measure the oil thickness in the two-layer model. The antenna is connected to the VNA using a coaxial cable, which is also calibrated using the ECal module. The antenna is placed on top of the modeled liquid layers and the reflection coefficient is measured and saved for another liquid modeled scenario, in order to define a mathematical calibration and measurement method based on the retrieved data. In the first scenario, the antenna has been accurately placed on the distilled water, using a prepared setup, as shown in Fig. 10(a), and then the reflection coefficient is generated by the VNA and was stored, as presented in Fig. 10(b). The next part of the experiment has focused on the addition of linseed oil with the container, to increase the oil thickness to 10 mm thickness, followed by saving and plotting the S_{11} values. The process is repeated for 20 and 30 mm oil thicknesses and the generated data are stored for the analysis, which has been shown in Fig. 10(c) and (d). The experimental magnitude of the first large transition point close to $f_c = 1.8$ GHz of the water is depicted in Fig. 10(b). The measured results have been compared with the simulations to determine the difference value, which refers to the difference between the simulation and experimental environments. This value for the magnitude has been found to be around 2.35 dB.

The procedure, namely, the calibration process, has been deployed, to subtract the value from the measured results compared with the simulated results. The measured S_{11} results for different oil layers are shown in Fig. 10(d).

This is effectively used to predict the first large transition points of the simulations, by simply subtracting the

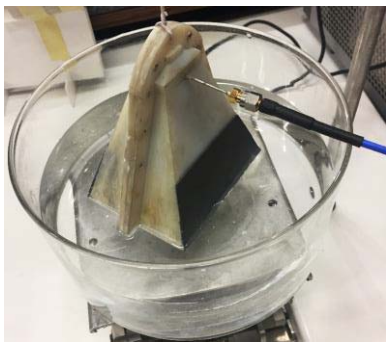

(a)

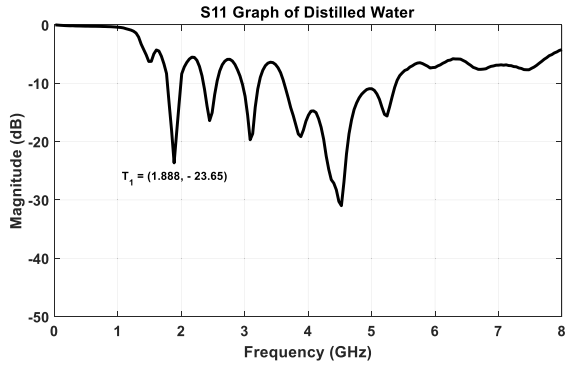

(b)

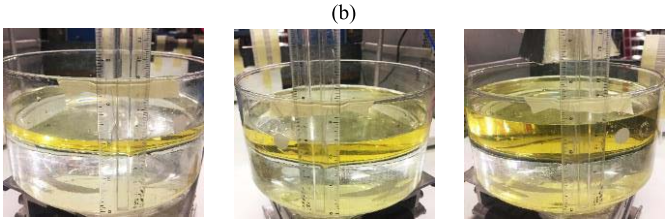

(c)

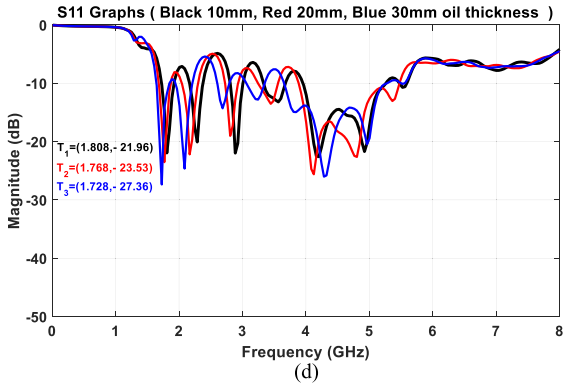

(d)

Fig. 10. (a) Prepared measurement setup, presenting the antenna placed on the distilled water for the experiment. (b) Measured S_{11} results of the antenna on the distilled water. (c) Prepared setup of the developed liquid model, for different oil thicknesses of 10–30 mm for the experiment. (d) Measured S_{11} results of the antenna for three developed cases, when the oil thicknesses are changed to 10, 20, and 30 mm.

magnitude rate. This has proved the output performance of the system based on both the numerical and measured results. This has shown that there is a negligible difference introduced into the system that could be the result of human errors.

C. Antenna Measurements on a Human Tissue

The proposed method presented above has been employed to accurately calibrate the system, followed by the measurement

(a)

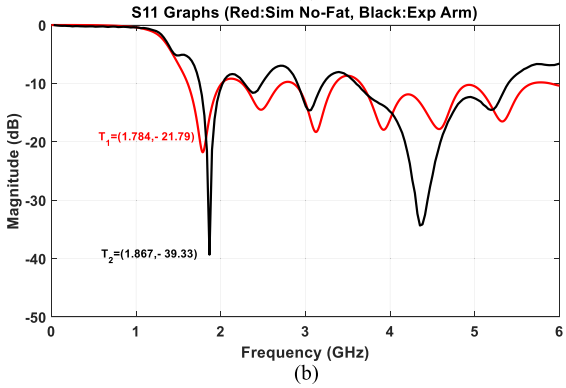

(b)

Fig. 11. (a) Developed antenna placed on the arm for the calibration. (b) Red plot presents the simulations (i.e., no fat case), and the black plot shows the measurements, obtained based on the arm case.

of the abdominal fat. Hence, the system has been appropriately calibrated using an area of the human body, where there is none or a small amount of fat exists, such as the arm, and the results have been further compared to the simulations with the same scenario (i.e., no fat layer exists model), as in Fig. 11(a).

The results exhibit a slight shift in magnitude and frequency, compared to the simulations, as can also be seen in Fig. 11(b). This minor difference could be due to the differences that may have been added to the system, during the experimental stage, as opposed to the error-free simulation environment.

It should be noted that the air gap between the antenna and the body has been eliminated by using the semisolid mixture, which has removed the effects of the air gap in the real experiment. In addition, the antenna has been placed on the abdominal area of the human body that had an unknown amount of fat, as presented in Fig. 12(a). Moreover, the S_{11} results are obtained based on the measurements on the body and are further compared with the measured results of the case based on the arm, as presented in Fig. 12(b).

In addition, the change in the magnitude at the highest point of the first large transition for the abdominal fat has been stored and calibrated using the simulations, to calculate the estimated amount of the fat in the abdominal. The highest point of the first large transition for the arm has been recorded at the frequency of 1.867 GHz, with a magnitude of -39.33 dB. In the abdominal case, the values are changed to 1.927 GHz with a magnitude of -22.15 dB. Also, the proposed method to calculate the estimated thickness of the oil layer has been used in this case, in order to accurately predict the fat thickness.

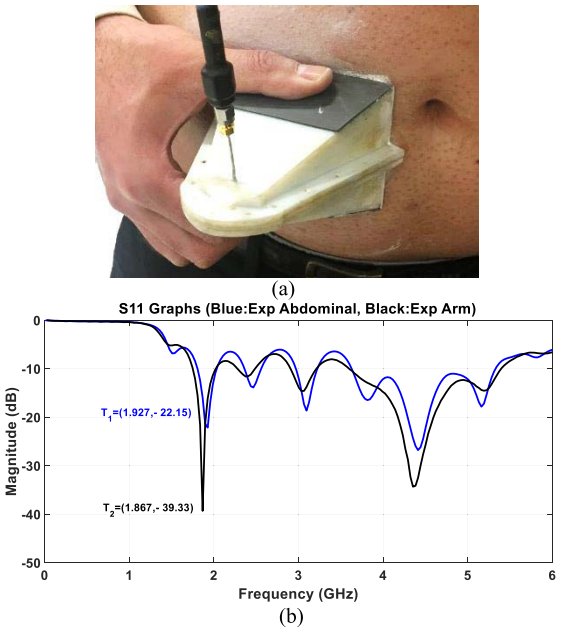

Fig. 12. (a) Antenna placed on the abdominal for the fat measurement. (b) Blue plot refers to the measured abdominal case, and the black plot refers to the measured arm case.

The first stage was to calibrate the measured magnitude of the first large transition point at the frequency of interest, according to the simulations given in Table III. By subtracting both the measured and simulated magnitude values, the value has been determined as −17.54 dB. This value is then added to the measured abdominal one to determine the magnitude value (i.e., −39.69 dB) of the real tissue, with respect to the simulation results. This value has been used in the equation of Fig. 8(e), to determine the fat thickness as 17.28 mm. The core of this work was conducted as part of the doctoral dissertation in [39].

V. Conclusion

This investigation has thoroughly presented the EM design and performance evaluations of a low cost and compact 3-D-printed PDRH antenna, filled with a low-conductive and high-dielectric oil and ceramic mixture. The primary objective of this work has been to determine and measure the abdominal fat thickness, based on a developed method, using the reflection coefficient response. The design of this novel antenna system incorporated the extension for locating the antenna close to the far-field region of the measured area, to enable the plane waves to penetrate more directive into the human body, and to introduce a delay to further resolve the overlapping issue. The microwave absorbing material has been also employed to extend a section of the design at the surface angles, where the ridges are located, to improve the directivity. The developed mixture exhibits a number of unique features, including the low conductivity and high permittivity, to be able to eliminate the air gap between the antenna and the body. The designed antenna operates in low frequencies to have a better penetration depth, along with a higher impedance matching due to the high-dielectric mixture. Lastly, a method has been developed to use the simulations of the reflection coefficients, as well as to determine and validate the fat thickness with respect to the measured results obtained during the experimental stages of the proposed system.

References

[1] K. L. Walton and V. C. Sundberg, "Broadband ridged horn design," *Microw. J.*, vol. 7, pp. 96–101, Apr. 1964.
[2] S. B. Cohn, "Properties of the ridge wave guide," *Proc. IRE*, vol. 35, no. 8, pp. 783–789, Aug. 1947.
[3] U. Schwarz, R. Stephan, and M. A. Hein, "Experimental validation of high-permittivity ceramic double-ridged horn antennas for biomedical ultra-wideband diagnostics," in *Proc. IEEE Int. Conf. Wireless Inf. Technol. Syst.*, Aug. 2010, pp. 1–4.
[4] D. T. Al-Zuhairi, J. M. Gahl, A. M. Abed, and N. E. Islam, "Characterizing horn antenna signals for breast cancer detection," *Can. J Elect. Compt. Eng.*, vol. 41, no. 1, pp. 8–16, Winter 2018.
[5] F. S. D. Clemente, M. Helbig, J. Sachs, U. Schwarz, R. Stephan, and M. A. Hein, "Permittivity-matched compact ceramic ultra-wideband horn antennas for biomedical diagnostics," in *Proc. Eur. Conf. Antennas Propag. (EuCAP)*, Apr. 2011, pp. 2386–2390.
[6] C. Bruns, P. Leuchtmann, and R. Vahldieck, "Analysis and simulation of a 1-18-GHz broadband double-ridged horn antenna," *IEEE Trans. Electromagn. Compat.*, vol. 45, no. 1, pp. 55–60, Feb. 2003.
[7] S. Kubota, X. Xiao, N. Sasaki, K. Kimoto, and T. Kikkawa, "Characteristics of UWB bow-tie antenna integrated with balun for breast cancer detection," in *Proc. IEEE Antennas Propag. Soc. Int. Symp.*, Jun. 2009, pp. 1–4.
[8] A. G. Dagheyan, A. Molaei, J. H. Juesas, and J. Martinez-Lorenzo, "Charachterization of two antipodal Vivaldi antennas for breast cancer near-field radar imaing," in *Proc. IEEE Int. Symp. Antennas Propag. (APSURSI)*, Fajardo, Puerto Rico, Jun. 2016, pp. 1481–1482.
[9] A. Khaleghi, I. Balasingham, and A. Vosoogh, "A compact ultra-wideband spiral helix antenna for in-body communications," in *Proc. 8th Eur. Conf. Antennas Propag. (EuCAP)*, Apr. 2014, pp. 3093–3096.
[10] S. Sarjoghian, Y. Alfadhl, and X. Chen, "On the limitation of ultra-wideband technique for medical scanning systems," in *Proc. Loughborough Antennas Propag. Conf. (LAPC)*, Nov. 2016, pp. 1–4.
[11] B. Zhang, Y.-X. Guo, H. Sun, and Y. Wu, "Metallic, 3D-printed, K-band-stepped, double-ridged square horn antennas," *Appl. Sci.*, vol. 8, no. 1, pp. 33–39, Dec. 2017.
[12] B. Majumdar, D. Baer, S. Chakraborty, K. P. Esselle, and M. Heimlich, "Additive manufacturing of a dual-ridged horn antenna," *Prog. Electromagn. Res. Lett.*, vol. 59, pp. 109–114, Apr. 2016.
[13] C. R. Garcia, H. H. Tsang, J. H. Barton, and R. C. Rumpf, "Effects of extreme surface roughness on 3D printed horn antenna," *Electron. Lett.*, vol. 49, no. 12, pp. 734–736, Jun. 2013.
[14] V. Midtboen, K. G. Kjelgard, and T. S. Lande, "3D printed horn antenna with PCB microstrip feed for UWB radar applications," in *Proc. IEEE MTT-S Int. Microw. Workshop Ser. Adv. Mater. Processes RF THz Appl. (IMWS-AMP)*, Pavia, Italy, Sep. 2017, pp. 1–3.
[15] U. Schwarz, R. Stephan, and M. A. Hein, "Miniature double-ridged horn antennas composed of solid high-permittivity sintered ceramics for biomedical ultra-wideband radar applications," in *Proc. IEEE Antennas Propag. Soc. Int. Symp.*, Jul. 2010, pp. 1–4.
[16] S. Latif, S. Pistorius, and L. Shafai, "A double-ridged horn antenna design in canola oil for medical imaging," in *Proc. 2nd Int. Conf. Adv. Electr. Eng. (ICAEE)*, Dec. 2013, pp. 421–424.
[17] S. I. Latif, L. Shafai, S. Pistorius, and D. Flores-Tapia, "Design and performance analysis of the miniaturised water-filled double-ridged horn antenna for active microwave imaging applications," *IET Microw., Antennas Propag.*, vol. 9, no. 11, pp. 1173–1178, Aug. 2015.
[18] S. Sarjoghian, M. H. Sagor, Y. Alfadhl, and X. Chen, "A 3D-printed high-dielectric filled elliptical double-ridged horn antenna for biomedical monitoring applications," *IEEE Access*, vol. 7, pp. 94977–94985, Jul. 2019.
[19] S. I. Latif, D. F. Tapia, D. R. Herrera, M. S. Nepote, S. Pistorius, and L. Shafai, "A directional antenna in a matching liquid for microwave radar imaging," *Int. J. Antennas Propag.*, vol. 2015, pp. 1–8, Oct. 2015.
[20] S. Klein *et al.*, "Waist circumference and cardiometabolic risk," *Diabetes Care*, vol. 30, no. 6, pp. 1647–1652, Jun. 2007.
[21] A. J. Dunkley, M. A. Stone, N. Patel, M. J. Davies, and K. Khunti, "Waist circumference measurement: Knowledge, attitudes and barriers in patients and practitioners in a multi-ethnic population," *Family Pract.*, vol. 26, no. 5, pp. 365–371, Oct. 2009.

[22] A.-K. Karlsson *et al.*, "Measurements of total and regional body composition in preschool children: A comparison of MRI, DXA, and anthropometric data," *Obesity*, vol. 21, no. 5, pp. 1018–1024, May 2013.
[23] T. Yoshizumi *et al.*, "Abdominal fat: Standardized technique for measurement at CT," *Radiology*, vol. 211, no. 1, pp. 283–286, Apr. 1999.
[24] M. D. Jensen, J. A. Kanaley, J. E. Reed, and P. F. Sheedy, "Measurement of abdominal and visceral fat with computed tomography and dual-energy X-ray absorptiometry," *Amer. J. Clin. Nutrition*, vol. 61, no. 2, pp. 274–278, Feb. 1995.
[25] H. R. Atta, *Ophthalmic Ultrasound—A Practical Guide*. Edinburgh. U.K.: Churchill Livingstone, Feb. 1996.
[26] C. Yu *et al.*, "Titanium dioxide engineered for near-dispersionless high terahertz permittivity and ultra-low-loss," *Sci. Rep.*, vol. 7, no. 1, p. 6639, Jul. 2017.
[27] T. S. Bird and A. W. Love, "Horn antennas," in *Antenna Engineering Handbook*, J. L. Volakis, Ed., 4th ed. New York, NY, USA: McGraw-Hill, ch. 14, Jan. 2007.
[28] E. Lier, "Review of soft and hard horn antennas, including metamaterial-based hybrid-mode horns," *IEEE Antennas Propag. Mag.*, vol. 52, no. 2, pp. 31–39, Apr. 2010.
[29] X. Yi, "Wireless antenna sensors for strain and crack monitoring," Ph.D. dissertation, Georgia Inst. Technol., Atlanta, GA, USA, 2014.
[30] A. R. R. Mallahzadeh, A. A. Dastranj, and H. R. Hassani, "Novel dual-polarized double-ridged horn antenna for wideband applications," *Prog. Electromag. Res.*, vol. 1, pp. 67–80, 2008.
[31] A. Mehrdadian, H. Fallahi, M. Kaboli, and S. A. Mirtaheri, "Design and implementation of 0.7 to 7 GHz broadband double-ridged horn antenna," in *Proc. 7th Int. Symp. Telecommun. (IST)*, Sep. 2014, pp. 250–255.
[32] C. A. Balanis, *Antenna Theory: Analysis and Design*, 4th ed. Hoboken, NJ, USA: Wiley, 2016.
[33] S. Sarjoghian, Y. Alfadhl, and X. Chen, "Compact ultra-wideband double-ridged horn antennas for medical imaging," in *Proc. Loughborough Antennas Propag. Conf. (LAPC)*, Nov. 2016, pp. 1–4.
[34] A. Rahimian, Q. H. Abbasi, A. Alomainy, and Y. Alfadhl, "A low-profile 28-GHz rotman lens-fed array beamformer for 5G conformal subsystems," *Microw. Opt. Technol. Lett.*, vol. 61, no. 3, pp. 671–675, Mar. 2019.
[35] H. Balegh, B. A. Arand, and L. Yousefi, "Side lobe level reduction in horn antennas using graphene," in *Proc. 24th Iranian Conf. Electr. Eng. (ICEE)*, May 2016, pp. 1937–1941.
[36] S. Sarjoghian, Y. Alfadhl, and X. Chen, "A novel wide-band reflection-based system for measuring abdominal fat in humans," in *Proc. URSI Int. Symp. Electromagn. Theory (EMTS)*, Aug. 2016, pp. 586–589.
[37] S. Alkaraki, Y. Gao, M. O. M. Torrico, S. Stremsdoerfer, E. Gayets, and C. Parini, "Performance comparison of simple and low cost metallization techniques for 3D printed antennas at 10 GHz and 30 GHz," *IEEE Access*, vol. 6, pp. 64261–64269, Nov. 2018.
[38] S. Rashid *et al.*, "3-D printed UWB microwave bodyscope for biomedical measurements," *IEEE Antennas Wireless Propag. Lett.*, vol. 18, no. 4, pp. 626–630, Apr. 2019.
[39] S. Sarjoghian, "Design and evaluation of microwave antennas for abdominal fat measurement systems," Ph.D. dissertation, School Elect. Eng. Comp. Sci., Queen Mary Univ. London, London, U.K., 2019.

Siamak Sarjoghian (Member, IEEE) received the B.Sc. (Hons.) and M.Sc. degrees in electrical and electronics engineering, and embedded and distributed systems from London South Bank University, London, U.K., in 2009 and 2010, respectively, and the Ph.D. degree in electronic engineering from the Queen Mary University of London, London, in 2019.

His research interests include antennas, bioelectromagnetics, microwaves, UWB, and embedded computing systems. He has authored or coauthored a number of articles in these areas.

Yasir Alfadhl (Senior Member, IEEE) received the B.Eng. degree (Hons.) in telecommunication engineering and the Ph.D. degree from the Queen Mary University of London (QMUL), London, U.K., in 2000 and 2006, respectively.

He is currently a Senior Lecturer (Associate Professor) with QMUL. He has authored over 100 articles in computational electromagnetics, electromagnetic propagation, high-power microwaves, bioelectromagnetics, and wireless communications. His research activities are focused on antennas and electromagnetic propagations, computational electromagnetics, and bioelectromagnetics.

Xiaodong Chen (Fellow, IEEE) is currently a Professor of microwave engineering with the School of Electronic Engineering and Computer Science, Queen Mary University of London (QMUL), London, U.K. He is also the Director of the Joint Research Laboratory on Electromagnetic Theory and Applications between QMUL and the Beijing University of Posts and Telecommunications, Beijing, China. He has coauthored 2 textbooks, over 100 journal articles, and 300 refereed conference articles. His research interests include microwave and THz antennas and devices, wireless communications, and bioelectromagnetics.

Clive G. Parini (Member, IEEE) received the B.Sc. (Eng) degree in electronic engineering and the Ph.D. degree from the Queen Mary University of London (QMUL), London, U.K., in 1973 and 1976, respectively.

He was with ERA Technology Ltd., Surrey, U.K. He joined QMUL, as a Lecturer, in 1977, where he became a Reader in 1990 and then a Professor in 1999, and is currently a Professor of antenna engineering and heads the Antenna & Electromagnetics Research Group. He has authored over 400 articles in research topics including array mutual coupling, array beam forming, antenna metrology, antennas for mobile and on-body communications, millimeter-wave compact antenna test ranges, millimeter-wave integrated antennas, quasi-optical systems, and antenna applications for metamaterials. He has authored the book entitled *Principles of Planar Near-Field Antenna Measurements* in 2008 and *Theory and Practice of Modern Antenna Range Measurements* in 2014.

Dr. Parini is a fellow of IET and a past Member and the Chairman of the IET Antennas & Propagation Professional Network Executive Team. He was elected as a fellow of the Royal Academy of Engineering in 2009. He is a past Member of the Editorial Board and a Past Honorary Editor of the *IET Microwaves, Antennas & Propagation*. He was one of the three coworkers to receive the IEE Measurements Prize for the work on near-field reflector metrology in 1990.